Strojniški vestnik - Journal of Mechanical Engineering 64(2018)10, 579-589
DOI:10.5545/sv-jme.2018.5339
Original Scientific Paper
Received for review: 2018-03-07
Received revised form: 2018-05-29
Accepted for publication: 2018-07-02

Force Control of Hydraulic Actuators using Additional Hydraulic Compliance

Job Angel Ledezma Pérez – Edson Roberto De Pieri – Victor Juliano De Negri*
Federal University of Santa Catarina, Brazil

This paper presents an approach for improving the performance of hydraulic force control systems by adding hydraulic compliance. Typically, force control systems require a flexible coupling system, such as a spring between the actuator and the load, to achieve a non-oscillatory response. To avoid the use of springs, this study proposes the use of special hoses to add compliance to the system hydraulically. With this approach, a direct connection between the actuator and the load is feasible, simplifying the mechanical assembly and saving physical space in the axial direction. An analytical model is proposed to estimate the appropriate hydraulic stiffness value and to select a commercial hose based on catalogue data. Moreover, a robust controller based on quantitative feedback theory is designed to improve the stability, performance and disturbance rejection of the force control system. The system performance is demonstrated by dynamic simulation and experimental results.

Keywords: hydraulic force control, hydraulic compliance, high expansion volumetric hose, QFT-based control

Highlights

- *A hydraulic force control system with added hydraulic compliance is presented.*
- *Passive compliance is provided with the use of hydraulic hoses instead of mechanical springs.*
- *An analytical procedure for selecting and sizing hydraulic hoses is proposed.*
- *The presented achievements are validated by dynamic simulation and experimental results.*

0 INTRODUCTION

Several industrial applications require controlled force for handling materials or machining tasks in which the end effector is in contact with the piece or equipment. In most cases, position/trajectory control is required at the same time as contact force control. Assembly of mechanical components, polishing and grinding of complex pieces, milling, and endurance tests are some examples for which there are demands for force-controlled actuators in substitution to manual work [1] and [2].

As discussed in [3], the problem of force control is more complex than the problem of position control, which often makes its practical implementation more difficult. In contrast, to force control systems, the dynamics of the load is not included in the closed-loop in the case of positioning systems, and thus good performance and disturbance rejection are more easily achieved.

One way to overcome the inherent problems associated with force control systems is by increasing the compliance. System compliance can be controlled or modified in active or passive ways [4] and [5]. Active compliance is obtained with force-based feedback control (software), allowing more flexibility to perform tasks for which compliance is required. Typically, this approach requires additional measuring for control and collision detection [6]. In contrast, passive compliance is typically obtained by introducing mechanical elastic components (hardware) between the actuator and the environment. This approach enables energy storage, and it is appropriate for safety applications [7]. The series elastic actuator (SEA) represents one well-known example of a passive compliance actuation system [8]. This kind of actuator has been applied to robotics and biomechanics due to its simplicity and good performance in force control [9] and [10]. In an SEA, a spring is placed between the actuator and the load, providing good force fidelity, low output impedance, and shock tolerance capability. However, the system bandwidth is reduced due to the use of this compliant element [8].

In addition to the use of a spring to increase the system compliance and improve the system performance, researchers have employed a spring as a simplified representation of the load. Good force responses have been obtained using control techniques such as nonlinear PD (proportional-derivative), fuzzy PID (proportional-integral-derivative), QFT (quantitative feedback theory), and backstepping [11] to [14]. References [15] and [16] included additional load motion measurements in order to cancel the disturbance characteristic and obtain better force tracking.

In contrast, the fluid compressibility in hydraulic actuators introduces a spring effect that is

*Corr. Author's Address: Federal University of Santa Catarina, Mechanical Engeeniring Department, LASHIP, Campus Universitário, Trindade, 88040-900, Florianópolis, SC, Brazil, victor.de.negri@ufsc.br

characterized by the hydraulic stiffness. This can be shaped by using hydraulic capacitive components such as flexible hoses or accumulators. The use of accumulators connected to the cylinder chambers has been described in conference papers and patents [17] to [19]. However, these publications do not take into account the mathematical modelling to determine the hydraulic compliance needed to achieve the force control requirements and select the hydraulic capacitive component.

In this context, the present paper introduces a pure hydro-elastic actuator (PHEA) that uses only hydraulic components to reduce the transmission stiffness. Mathematical modelling and analysis are carried out, and a procedure for sizing the required hydraulic components in order to increase the compliance is determined. Instead of accumulators, the use of hoses with high volumetric expansion (HVE) is investigated.

Considering the effects of compliance addition and the possible parametric variations of the system, this paper considers the use of a robust controller based on the quantitative feedback theory (QFT) technique [20]. Furthermore, the load is assumed to be continuously in contact with the actuator, and the load-displacement acts as a disturbance over the force control system.

The following section provides a brief description of the hydraulic force control system. The nonlinear and linear modelling is presented in Section 2 followed by the proposed method for determining the hydraulic stiffness. The force controller based on the QFT technique is then designed, and simulation and experimental results are discussed. The last section presents the conclusions.

1 THE FORCE CONTROL SYSTEM

A hydraulic actuation system is very stiff due to the low fluid compressibility. Direct contact between the cylinder and the load would cause the entire system to be stiffer, and even a small control signal sent to a servovalve could generate large force variations due to the high open-loop gain.

Reference [21] emphasizes the advantages of including a spring in a force control system. In [8], the procedure of the spring selection for the SEA was improved by using two types of linear actuators: an electromechanical and a hydraulic actuator. In both cases, the introduction of a compliant element between the actuator and the load decreases the output impedance. Additionally, the measurement of the spring compression is used to calculate indirectly the force applied over the load (Fig. 1a).

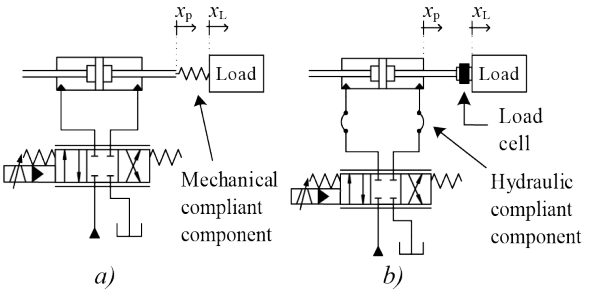

Fig. 1. *Compliance addition in a hydraulic force system using a) spring and b) HVE hoses*

The use of the spring limits the rate of the force applied by the hydraulic actuator, ensuring some degree of isolation between the hydraulic system and the movement of the load (environment) and maintaining a stable and robust applied force.

The use of a hydraulic compliant component instead of a spring is proposed. Fig. 1b shows an option using high volumetric expansion (HVE) hoses between the servovalve and cylinder. The use of accumulators instead of hoses could also be possible for similar purposes.

2 MATHEMATICAL MODELING

Two mathematical models are explained in this section: a nonlinear model, which is used for simulation in order to obtain force responses; and a linear model, used for the controller design and hose sizing. Both models are based on Fig. 1b.

2.1 Nonlinear Modelling of the Hydraulic System

2.1.1 Servovalve Modelling

In the design of the hydraulic circuit, a symmetrical servovalve is used (Fig. 2) [22]. The dynamic relationship between the input control signal (U_C) and the spool displacement, represented by an equivalent voltage (U_{Csp}), can be approximated by a second-order function:

$$U_C = \frac{1}{\omega_{nv}{}^2}\frac{d^2U_{Csp}}{dt^2} + \frac{2\xi_v}{\omega_{nv}}\frac{dU_{Csp}}{dt} + U_{Csp}, \qquad (1)$$

where ω_{nv} is the natural frequency of the valve and ξ_v represents the damping ratio of the valve.

The flow rate through the valve, including the effects of internal leakage can be described by the

following equations [23], where a control signal range of –10 V to +10 V is assumed:

- for $U_{\mathrm{Csp}} \geq 0$:

$$q_{v\mathrm{A}} = \left(K_{v\mathrm{p}} \frac{U_{\mathrm{Csp}}}{U_{\mathrm{Cn}}} + K_{v\mathrm{inp}} \right) \sqrt{p_{\mathrm{S}} - p_{\mathrm{A}}} - K_{v\mathrm{inp}} \sqrt{p_{\mathrm{A}} - p_{\mathrm{T}}}, \quad (2)$$

$$q_{v\mathrm{B}} = \left(K_{v\mathrm{p}} \frac{U_{\mathrm{Csp}}}{U_{\mathrm{Cn}}} + K_{v\mathrm{inp}} \right) \sqrt{p_{\mathrm{B}} - p_{\mathrm{T}}} - K_{v\mathrm{inp}} \sqrt{p_{\mathrm{S}} - p_{\mathrm{B}}}, \quad (3)$$

- for $U_{\mathrm{Csp}} < 0$:

$$q_{v\mathrm{A}} = -\left(K_{v\mathrm{p}} \frac{|U_{\mathrm{Csp}}|}{U_{\mathrm{Cn}}} + K v_{v\mathrm{inp}} \right) \sqrt{p_{\mathrm{A}} - p_{\mathrm{T}}} + K_{v\mathrm{inp}} \sqrt{p_{\mathrm{S}} - p_{\mathrm{A}}}, \quad (4)$$

$$q_{v\mathrm{B}} = -\left(K_{v\mathrm{p}} \frac{|U_{\mathrm{Csp}}|}{U_{\mathrm{Cn}}} + K_{v\mathrm{inp}} \right) \sqrt{p_{\mathrm{S}} - p_{\mathrm{B}}} + K_{v\mathrm{inp}} \sqrt{p_{\mathrm{B}} - p_{\mathrm{T}}}, \quad (5)$$

where $q_{v\mathrm{A}}$ and $q_{v\mathrm{B}}$ are the flow rates at ports A and B, respectively; p_{A} and p_{B} are the pressures in lines A and B, respectively; p_{S} and p_{T} represent the supply and the reservoir pressures, respectively; U_{Cn} is the nominal control signal. $K_{v\mathrm{p}}$ is the partial flow coefficient of the valve; and $K_{v\mathrm{inp}}$ is the internal partial leakage coefficient.

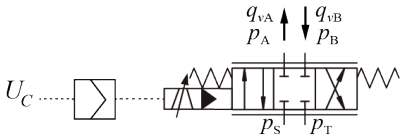

Fig. 2. *Flow rates and pressures at the servovalve*

2.1.2 Cylinder Modelling

Considering Fig. 3 and applying the continuity equation for each cylinder chamber yields:

$$q_{v\mathrm{A}} = A_{\mathrm{A}} \frac{\mathrm{d}x_{\mathrm{p}}}{\mathrm{d}t} + \frac{V_{\mathrm{A}}}{\beta_{\mathrm{e}}} \frac{\mathrm{d}p_{\mathrm{A}}}{\mathrm{d}t}, \quad (6)$$

and

$$q_{v\mathrm{B}} = A_{\mathrm{B}} \frac{\mathrm{d}x_{\mathrm{p}}}{\mathrm{d}t} - \frac{V_{\mathrm{B}}}{\beta_{\mathrm{e}}} \frac{\mathrm{d}p_{\mathrm{B}}}{\mathrm{d}t}, \quad (7)$$

where A_{A} and A_{B} are the piston areas in chambers A and B, respectively; x_{p} represents the piston displacement, and β_{e} is the effective bulk modulus.

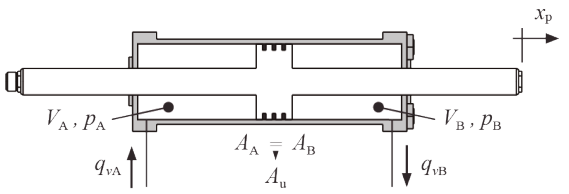

Fig. 3. *Variables and parameters of the cylinder*

The displacement of the rod can be modelled using Newton's second law:

$$F_{\mathrm{H}} - F_{\mathrm{fr}} - F_{\mathrm{e}} = M \frac{\mathrm{d}^2 x_{\mathrm{p}}}{\mathrm{d}t^2}, \quad (8)$$

where $F_{\mathrm{H}} = p_{\mathrm{A}} A_{\mathrm{A}} - p_{\mathrm{B}} A_{\mathrm{B}}$ is the hydraulic force, F_{fr} represents the friction force, F_{e} is the applied force, and M is the piston mass. In turn, the force applied over the load can be represented as:

$$F_{\mathrm{e}} = K_{\mathrm{S}} \left(x_{\mathrm{p}} - x_{\mathrm{L}} \right), \quad (9)$$

such that K_{S} is the load cell stiffness and x_{L} represents the load displacement.

2.2 Linear Modelling of the Hydraulic System

2.2.1 Servovalve Modelling

The flow rate through the valve (Eqs. (2) to (5)), linearized for any $U_{\mathrm{Csp}i}$ and $p_{\mathrm{L}i}$, can be represented as:

$$q_{v\mathrm{C}} = K_{q\mathrm{U}i} U_{\mathrm{Csp}} - K_{ci} p_{\mathrm{L}}, \quad (10)$$

where:

$$K_{q\mathrm{U}i} = \left(\frac{K_{v\mathrm{p}}}{U_{\mathrm{Cn}}} \right) \sqrt{\left(p_{\mathrm{S}} - p_{\mathrm{T}} - \mathrm{sgn}(U_{\mathrm{Csp}}) p_{\mathrm{L}i} \right) / 2}, \quad (11)$$

and

$$K_{ci} = \frac{K_{v\mathrm{p}}}{\sqrt{8}} \frac{|U_{\mathrm{Csp}i}|}{U_{\mathrm{Cn}}} \sqrt{\frac{1}{p_{\mathrm{S}} - p_{\mathrm{T}} - \mathrm{sgn}(U_{\mathrm{Csp}i}) p_{\mathrm{L}i}}} + \frac{K_{v\mathrm{inp}}}{\sqrt{8}} \left(\sqrt{\frac{1}{p_{\mathrm{S}} - p_{\mathrm{T}} - \mathrm{sgn}(U_{\mathrm{Csp}i}) p_{\mathrm{L}i}}} + \sqrt{\frac{1}{p_{\mathrm{S}} - p_{\mathrm{T}} + \mathrm{sgn}(U_{\mathrm{Csp}i}) p_{\mathrm{L}i}}} \right), \quad (12)$$

such that $K_{q\mathrm{U}i}$ is the flow-voltage gain at operating point i; K_{ci} the flow-pressure coefficient at operating point i; $p_{\mathrm{L}} = p_{\mathrm{A}} - p_{\mathrm{B}}$ the load pressure; and $q_{v\mathrm{C}}$ the control flow rate considered as the average of the $q_{v\mathrm{A}}$ and $q_{v\mathrm{B}}$.

2.1.2 Cylinder Modelling

Since the total variation of volume is the same for the two chamber volumes, it is possible to substitute V_A and V_B in Eqs. (6) and (7) with the parametric uncertainty V. This approach is suitable for the use of the quantitative feedback theory (QFT). Therefore, the hydraulic stiffness (K_H) can be generalized as:

$$K_H = \frac{\beta_e A_A^2}{V_A} + \frac{\beta_e A_B^2}{V_B} = \frac{2\beta_e A_u^2}{V}, \tag{13}$$

and the linear model of the symmetrical cylinder results:

$$q_{vC} = A_u \frac{dx_p}{dt} + \frac{A_u^2}{K_H}\frac{dp_L}{dt}, \tag{14}$$

where $A_u = A_A = A_B$ is the useful area of the piston.

The friction force is a nonlinear function of velocity and can be described by a variable viscous friction coefficient (f_v) [24]. This coefficient can be considered as an uncertain parameter, and this assumption allows the motion equation to become linear, yielding:

$$A_u p_L - f_v \frac{dx_p}{dt} - F_e = M \frac{d^2 x_p}{dt^2}. \tag{15}$$

2.3 Open Loop Transfer Function

For the open-loop (OL) transfer function, the values of K_{qUi} and K_{ci} are considered to be evaluated at null operating point ($i = 0$), where $U_{Csp0} = 0$, $q_{vC0} = 0$, and $p_{L0} = 0$.

Combining Eqs. (1), (9), (10) and (14) with (15), the OL transfer function that relates the output force (F_e) to the input control signal (U_C) and the load displacement (x_L) is:

$$F_e(s) = \frac{c_0 U_C(s)}{a_5 s^5 + a_4 s^4 + a_3 s^3 + a_2 s^2 + a_1 s + a_0} - \frac{K_S\left(b_4 s^4 + b_3 s^3 + b_2 s^2 + b_1 s + b_0\right) s X_L(s)}{a_5 s^5 + a_4 s^4 + a_3 s^3 + a_2 s^2 + a_1 s + a_0}, \tag{16}$$

where:

$a_0 = \omega_{nv}^2 K_{c0} K_H K_S$,

$a_1 = \omega_{nv}^2 A_u^2 (K_H + K_S) + K_{c0} K_H (2\xi_v \omega_{nv} K_S + \omega_{nv}^2 f_v)$,

$a_2 = 2\xi_v \omega_{nv} A_u^2 (K_H + K_S) + \omega_{nv}^2 A_u^2 f_v + K_{c0} K_H (2\xi_v \omega_{nv} f_v + \omega_{nv}^2 M + K_S)$,

$a_3 = 2\xi_v \omega_{nv} A_u^2 f_v + \omega_{nv}^2 A_u^2 M + K_{c0} K_H (2\xi_v \omega_{nv} M + f_v) + A_u^2 (K_H + K_S)$,

$a_4 = 2\xi_v \omega_{nv} A_u^2 M + A_u^2 f_v + K_{c0} K_H M$,

$a_5 = A_u^2 M$,

$b_0 = \omega_{nv}^2 A_u^2 K_H + \omega_{nv}^2 f_v K_{c0} K_H$,

$b_1 = 2\xi_v \omega_{nv} A_u^2 K_H + \omega_{nv}^2 A_u^2 f_v + K_{c0} K_H (2\xi_v \omega_{nv} f_v + \omega_{nv}^2 M)$,

$b_2 = 2\xi_v \omega_{nv} A_u^2 f_v + \omega_{nv}^2 A_u^2 M + A_u^2 K_H + K_{c0} K_H (2\xi_v \omega_{nv} M + f_v)$,

$b_3 = 2\xi_v \omega_{nv} A_u^2 M + A_u^2 f_v + K_{c0} K_H M$,

$b_4 = A_u^2 M$,

$c_0 = A_u K_H K_{qU0} K_S \omega_{nv}^2$.

3 SELECTION OF THE HYDRAULIC HOSE

In this section, a procedure for sizing the hydraulic hose required to add hydraulic compliance to the system is proposed. It consists of a few analytical expressions that allow the selection of commercial HVE hoses in a simple way. To demonstrate its effectiveness, dynamic responses using the nonlinear model as well as experimental results are reported in Section 5.

3.1 Selecting the Desired Hydraulic Stiffness

Based on Eq. (16), and expressing the input control signal $U_C(s)$ as $G(s)(F_{ref}(s) - F_e(s))$, where $G(s)$ and $F_{ref}(s)$ represent the controller transfer function and the reference force, respectively, the closed-loop (CL) transfer function results in:

$$F_e(s) = \frac{G(s)N_1(s)}{D(s) + G(s)N_1(s)} F_{ref}(s) - \frac{N_2(s)}{D(s) + G(s)N_1(s)} X_L(s), \tag{17}$$

where:

$N_1(s) = c_0$,

$N_2(s) = K_S (b_4 s^4 + b_3 s^3 + b_2 s^2 + b_1 s + b_0)\, s$,

$D(s) = a_5 s^5 + a_4 s^4 + a_3 s^3 + a_2 s^2 + a_1 s + a_0$.

The first part of Eq. (17) determines the system performance in response to a reference force. The second part of Eq. (17) describes how the system behaves when a disturbance input $X_L(s)$ occurs. Therefore, it is related to the output impedance and can be considered as a measure of the system's capability against external disturbances.

The hydraulic stiffness K_H affects both parts of Eq. (17) as reported below. Therefore, the hose selection will be based on a trade-off between performance and disturbance rejection.

3.1.1 Output Impedance

The output impedance can be analysed considering the transfer function $F_e(s)/X_L(s)$ presented in the second part of Eq. (17). The presence of a zero at the origin introduces an implicit disturbance rejection. However,

based on the initial value theorem, an initial overshoot equal to the equivalent stiffness ($K_H K_S/(K_H+K_S)$) times a disturbance amplitude is expected.

Therefore, increasing the rejection capability against load movement requires that K_H is as low as possible. Nevertheless, this value must be greater than or equal to the hydraulic stiffness required to achieve the required performance, which is discussed next.

3.1.2 Desired Tracking Control Ratio

An approximation of the first part of Eq. (16) expressed by first and second order terms can be written as:

$$\frac{F_e(s)}{U_C(s)} = \left(\frac{K_{qU0}K_{eq}/A_u}{s+K_{c0}K_{eq}/A_u^2}\right)\left(\frac{d_0}{s^2+d_1 s+d_0}\right) \cdot \left(\frac{e_0}{s^2+e_1 s+e_0}\right), \quad (18)$$

where:

$d_0 = (K_H + K_S)/M$,
$d_1 = f_v/M$,
$e_0 = \omega_{nv}^2$,
$e_1 = 2\xi_v\omega_{nv}$,
$K_{eq} = K_S K_H/(K_S+K_H)$, representing the equivalent stiffness.

The first term is equivalent to a linear modelling of the open-loop system neglecting mass, friction and valve dynamics. The middle term is related to Newton's second law including the effect of the hydraulic stiffness. Finally, the last term represents the servovalve dynamics.

It is noteworthy that, using the parameters presented in the Appendix, Eq. (18) is an almost exact approximation of Eq. (16), with a maximum difference between curves of 0.2 dB in magnitude and 0.003º in phase.

The open loop poles of Eq. (18) are shown in Table 1. for different hydraulic stiffness values for which K_{Hn} corresponds to the nominal stiffness when using rigid pipes (instead of hoses). The real pole related to the hydraulic subsystem is $-K_{c0}K_{eq}/A_u^2$, and it is dominant over the other two complex poles. This fact becomes more noticeable as the hydraulic stiffness is reduced. The damped natural frequency of the mechanical subsystem is loosely influenced by the hydraulic stiffness variation.

Due to the dominance of the real pole, the first term in Eq. (16) can be substituted by the first order term in Eq. (18) and the corresponding closed-loop transfer function is:

$$\frac{F_e(s)}{F_{ref}(s)} = \frac{G(s)(K_{qU0}K_{eq}/A_u)}{s+(K_{c0}K_{eq}/A_u^2)+G(s)(K_{qU0}K_{eq}/A_u)}. \quad (19)$$

Table 1. *Pole locations for different values of K_H*

K_H [N/m]	Hydraulic dynamics $\frac{K_{qU0}K_{eq}/A_u}{(s+K_{c0}K_{eq}/A_u^2)}$	Mechanical dynamics $\frac{d_0}{(s^2+d_1 s+d_0)}$	Servovalve dynamics $\frac{e_0}{(s^2+e_1 s+e_0)}$
$K_{Hn} = 1.5\times10^7$	–2.963	$-11.6 \pm 2.93\times10^3$i	-989 ± 479i
0.1 K_{Hn}	–0.336	$-11.4 \pm 2.75\times10^3$i	-989 ± 479i
0.01 K_{Hn}	–0.034	$-11.4 \pm 2.73\times10^3$i	-989 ± 479i

A desired tracking control ratio for the system can be specified by:

$$F_e(s)/F_{ref}(s) = K_{SS}/(\tau_d s+1), \quad (20)$$

where K_{SS} is the steady-state gain, and τ_d is the desired time constant.

Comparing Eqs. (19) and (20) and assuming a proportional controller, a correlation between the required hydraulic stiffness and the proportional gain (K_p) can be obtained:

$$K_H = \frac{K_S A_u^2}{K_S\tau_d(K_{c0}+A_u K_p K_{qU0})-A_u^2}. \quad (21)$$

3.2 Selecting a Commercial Hydraulic Hose

The hose diameter can be calculated based on the maximum flow rate (q_{vmax}) and the recommended fluid velocity in the hose (v_{oil}) according to:

$$D_{ho} = \sqrt{4q_{vmax}/\pi v_{oil}}. \quad (22)$$

Hose manufacturers recommend using fluid velocities of 2 m/s to 4 m/s for pressure lines [25] and [26]. Given that $A_u = A_A = A_B$, the maximum and minimum values for hydraulic stiffness (K_H) can be expressed by:

$$K_{Hmax} = \frac{\beta_e A_u^2 (A_u L + 2V_{ho})}{V_{ho}(A_u L + V_{ho})} \Rightarrow \text{ at } x_p = 0 \text{ or } x_p = L, \quad (23)$$

and

$$K_{Hmin} = \frac{4\beta_e A_u^2}{A_u L + 2V_{ho}} \Rightarrow \text{ at } x_p = \frac{L}{2}, \quad (24)$$

where V_{ho} represents the volume of oil trapped in the hose coupled to each cylinder chamber, and L is the

piston stroke. For simplification, henceforth Eq. (24) will be used for the calculation of K_H.

The effective bulk modulus can be represented as:

$$\beta_e = \frac{\beta_0 \beta_{ho}}{\beta_0 + \beta_{ho}} = \frac{r_\beta \beta_0 \beta_{hoSS}}{\beta_0 + r_\beta \beta_{hoSS}}, \quad (25)$$

where β_o is the fluid bulk modulus, β_{ho} represents the dynamic hose bulk modulus, β_{hoSS} is the static hose bulk modulus, and r_β is the ratio β_{ho}/β_{hoSS}.

According to **[27]**, the hose bulk modulus changes during the system operation, i.e., dynamic bulk modulus (β_{ho}) is higher than static bulk modulus (β_{hoSS}) due to a phenomena called dynamic hardening. Those authors state that the r_β is about 4 to 5 for nylon braid hoses, which is the case of the HVE hoses used in this paper.

According to the experimental results presented in **[27]**, the static hose bulk modulus can be expressed by:

$$\beta_{hoSS} = \left(1 + \frac{\Delta V_{ho}}{V_{0ho}}\right) \frac{dp}{d\left(\frac{\Delta V_{ho}}{V_{0ho}}\right)}, \quad (26)$$

where ΔV_{ho} represents the change in the hose volume, V_{0ho} is the initial volume of the hose, and p is the working pressure.

This equation can be rewritten in order to calculate β_{hoSS} as a function of hose catalogue data, yielding:

$$\beta_{hoSS} = \frac{\left(A_{ho} + E\right)}{\varepsilon} = \frac{\left(\pi D_{ho}^{\,2} + 4E\right)}{4\varepsilon}, \quad (27)$$

where E represents the volumetric expansion of the hose, defined as $\Delta V_{ho}/L_{ho}$, being L_{ho} the hose length; D_{ho} is the hose diameter, and ε corresponds to dE/dp.

E is a parameter determined at the working pressure (p), and ε can be assumed constant for a specific hose, corresponding to the slope of straight lines in graphs of E versus p provided by manufacturers **[25]** and **[26]**. Combining Eqs. (24), (25) and (27) yields:

$$L_{ho} = \frac{8 A_u^{\,2} r_\beta \beta_0 \left(\pi D_{ho}^{\,2} + 4E\right)}{\pi D_{ho}^{\,2} K_H \left(4\varepsilon\beta_0 + r_\beta \left(\pi D_{ho}^{\,2} + 4E\right)\right)} - \frac{2 A_u L}{\pi D_{ho}^{\,2}}. \quad (28)$$

Eq. (28) shows that to obtain smaller hydraulic stiffness K_H, longer hose L_{ho} is required. Furthermore, the greater the hose's volumetric expansion, the lower the hose length to achieve the same hydraulic stiffness.

If necessary, the process of hose selection using Eqs. (21) and (28) can be iterative to avoid obtaining long hoses, which may not be suitable for implementation. For example, if a calculated hydraulic stiffness results in a long hose, the proportional gain can be decreased in Eq. (21), resulting in a higher K_H and smaller L_{ho}. Therefore, the final value of hydraulic stiffness is obtained from a trade-off between K_H, K_p, and L_{ho}.

In contrast, Eq. (28) can also be used to calculate K_H based on a pre-selected hose with the required D_{ho} (from Eq. (22)) and the desired L_{ho}. After that, the proportional gain to achieve the required closed loop response can be calculated by isolating it in Eq. (21).

The use of a proportional controller in this design stage allows obtaining a very good approximation for the required hydraulic stiffness. A specific controller design and the system dynamic analysis using a nonlinear model can then be carried out as shown in Sections 5 and 6.

3.3 Example of Hose Selection

Consider a Pure Hydro-Elastic Actuator (PHEA), as shown in Fig. 1b, able to apply forces up to 9000 N. The desired tracking control ratio is specified according to Eq. (20) with a time constant τ_d equal to 50 ms. The system parameters are according to the Appendix, with K_{qU0} and K_{c0}, calculated at null operating based on Eqs. (11) and (12).

Considering the maximum flow rate equal to the test rig pump supply (1.6×10^{-4} m^3/s) and fluid velocity in the line equal to 2 m/s, a commercial hose diameter of 12.7 mm (1/2 in) was selected using Eq. (22). Analysing HVE hose catalogues, the EATON Synflex ® 3130-08 was selected **[25]**. The hose volumetric expansion is 1.56×10^{-5} m^3/m @ 7×10^6 Pa (4.7 cc/ft @ 1000 psi), resulting in a static bulk modulus (β_{hoSS}) of 6.36×10^7 Pa. Based on Eq. (26), an r_β value equal to 5 was considered.

As discussed before, the system performance must be determined by a trade-off between K_H, K_p, and L_{ho}. In this study, a L_{ho} equal to 1.5 m was specified and using Eq. (28) the resulting K_H is 2.24×10^6 N/m and, based on Eq. (21), K_p is 2.7×10^{-4}.

The hydraulic force control system according to the configuration shown in Fig. 1b was assembled in a test rig as shown in Fig. 4. The system comprises two hoses interconnecting each cylinder chamber with the servovalve. A load cell is fixed at the cylinder rod, and it will be in contact with a metal block attached to the test rig frame. The parameter values of this experimental setup are presented in the Appendix. For the QFT controller design and dynamic simulation, K_S equal to 2×10^7 N/m was used, corresponding to the

equivalent stiffness resulting from the load cell and environment compliances.

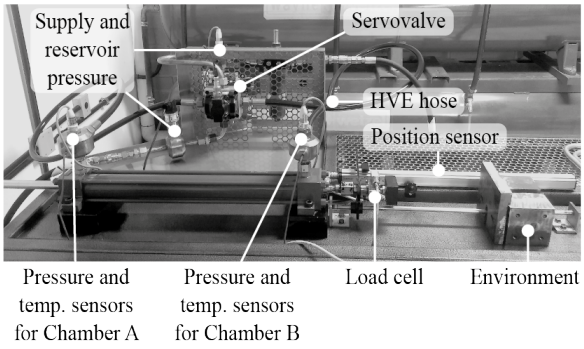

Fig. 4. *Hydraulic test bench used for experiments*

4 CONTROLLER DESIGN USING LINEAR QFT

The QFT allows designing a linear controller for a nonlinear system, assuming it as linear under the effect of disturbances and parametric variations [20]. In this study, the controller design was carried out using the QFT frequency domain control design toolbox for use with Matlab [28]. The objective of the QFT-based control design is to synthesize a prefilter ($F(s)$) and a controller ($G(s)$) such that the force responses of the system always fall within a predefined time-domain tolerance described by upper and lower limits.

Typically, these limits are based on second-order specifications, such that the time constant value (τ_d = 50 ms) used at the hose selection procedure (Section 3.1.2) is converted on a settling time ($t_{S1\%}$ = 200 ms). In this study, the upper and lower limits were defined as:

- Upper Limit ($B_U(t)$): settling time ($t_{S1\%}$) of 0.1 s and maximum overshoot of 1 %.
- Lower limit ($B_L(t)$): settling time ($t_{S1\%}$) of 0.3 s without overshoot.

Translating the specifications from the time domain to the frequency domain yields:

$$T_{rU}(s)=\left(\frac{2116}{s^2+73.6s+2116}\right)\left(\frac{s+75}{75}\right), \quad (29)$$

and

$$T_{rL}(s)=\left(\frac{400}{s^2+40s+400}\right)\left(\frac{50}{s+50}\right). \quad (30)$$

The addition of a zero and a pole in Eqs. (29) and (30), respectively, relax the requirements for the controller design in the frequency domain without affecting the responses in the time domain.

Table 2 shows the parametric uncertainties assumed in the plant model described by Eq. (16).

Table 2. *Parameter uncertainties at Eq. (16)*

Description	Nominal value	Range
f_v [Ns/m]	100	100 to 3×10^4
K_{qUi} [m^3/(s·V)]	5.4×10^{-5}	3.23×10^{-5} to 5.61×10^{-5}
K_{ci} [m^3/(s·Pa)]	6.42×10^{-13}	6.42×10^{-13} to 7×10^{-11}
K_H [N/m]	2.24×10^6	2.24×10^6 to 4.11×10^6
ω_{nv} [rad/s]	1099	879 to 1319
ξ_v	0.9	0.72 to 1.08

To define the uncertainties, the following considerations were assumed:

- f_v varies from a minimum value related to the Coulomb friction to a maximum value representing the stiction, which was obtained experimentally,
- the range of parametric uncertainty for K_{qUi} was calculated using Eq. (11), assuming no load (p_{Li}=0) and the operating point at the maximum power (p_{Li}=2p_S/3). The nominal value was obtained through experiments according to ISO 10770-1 [29],
- the range for K_{ci} was calculated using Eq. (12). The nominal value was obtained based on the results of the internal leakage measurement test according to ISO 10770-1 [29],
- K_H varies from the minimum to maximum hydraulic stiffness calculated by Eqs. (23) and (24),
- Finally, a ±20% variation around the nominal values extracted from the catalogue is assumed for ω_{nv} and ξ_v.

The other parameter values used for the controller design are shown in the Appendix, with the exception of K_S that was changed in order to represent the equivalent stiffness instead of just the load cell characteristic. Based on the measurement of the environment deflection, the resulting Ks was 2×10^7 N/m.

For the QFT boundary generation, robust stability, disturbance rejection and reference tracking criteria are considered in this study.

The robust stability bounds are defined through [20]:

$$\left|T_1(j\omega)\right|=\left|\frac{P(j\omega)G(j\omega)}{1+P(j\omega)G(j\omega)}\right|=\left|\frac{L(j\omega)}{1+L(j\omega)}\right| \le \delta_1(\omega)=1.3, \quad \omega\in\Omega_1, \quad (31)$$

where $P(j\omega)$ represents the plant, $G(j\omega)$ represents the controller, $L(j\omega)$ is known as the loop transmission function, and $\delta_1(\omega)$ is a constant constraint calculated assuming a gain margin of 5 dB. The subset of analysis frequencies Ω_1 is {0.01, 0.1, 1, 5, 10, 50, 100, 150} rad/s.

For the disturbance rejection bounds, the constraint function $\delta_2(\omega)$ represents the disturbance control ratio:

$$\left|T_2(j\omega)\right| = \left|\frac{Y(j\omega)}{D(j\omega)}\right| = \left|\frac{1}{1+L(j\omega)}\right| \leq \delta_2(\omega) = \frac{s}{s+15}, \quad \omega \in \Omega_2, \tag{32}$$

where $Y(j\omega)$ represents the output, $D(j\omega)$ is the disturbance signal, and the subset of analysis frequencies Ω_2 is {0.01, 0.1, 1, 5, 10} rad/s.

Finally, the reference tracking bounds are defined as:

$$\delta_{5\text{inf}}(\omega) \leq \left|T_5(j\omega)\right| = \left|\frac{Y(j\omega)}{R(j\omega)}\right| = \left|F(j\omega)\frac{L(j\omega)}{1+L(j\omega)}\right| \leq \delta_{5\text{sup}}(\omega), \quad \omega \in \Omega_5, \tag{33}$$

where $R(j\omega)$ is related to the reference signal, $F(j\omega)$ represents the prefilter, and the constraint functions $\delta_{5\text{sup}}(\omega)$ and $\delta_{5\text{inf}}(\omega)$ are the transfer functions $T_{\text{rU}}(s)$ and $T_{\text{rL}}(s)$ defined in equations (29) and (30), respectively. The subset of analysis frequencies Ω_5 is {0.01, 0.1, 1, 5, 10, 50, 100, 150} rad/s.

After the bound generation and intersection, the loop shaping process is carried out to obtain the controller function (Fig. 5) **[20]**.

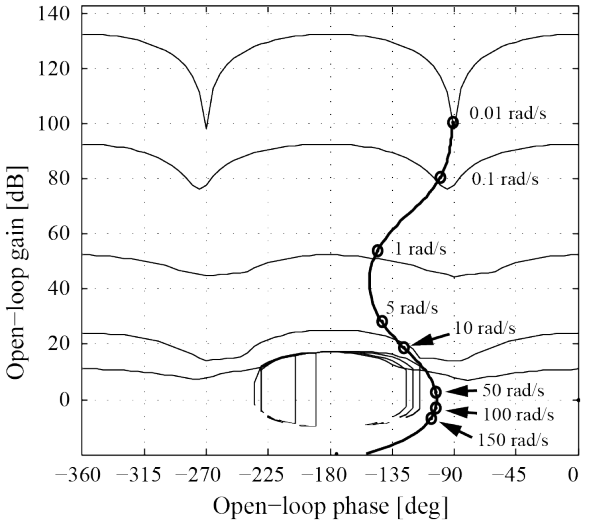

Fig. 5. *Loop shaping of the controller*

The resulting controller is:

$$G(s) = \left(0.001s + 0.008\right)/s. \tag{34}$$

The synthesis of the prefilter is similar to that of the controller, resulting in:

$$F(s) = 910/(s^2 + 83s + 910). \tag{35}$$

The hydraulic force control system, including the prefilter and controller, was implemented in Simulink, using the block diagram shown in Fig. 6.

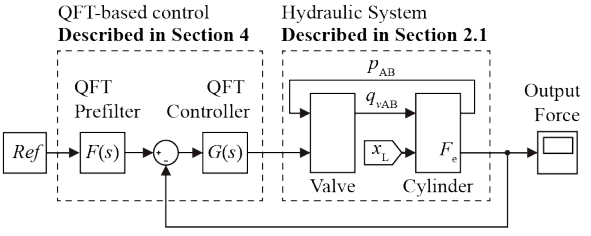

Fig. 6. *Block diagram of the hydraulic force control system*

5 EXPERIMENTAL AND SIMULATION RESULTS

Experimental tests and simulations were carried out using the selected HVE hose according to Section 3.3. A force-tracking reference was defined as several force steps of different magnitudes (Fig. 7a). To show that the model used for simulation has a good matching with the experimental results, an enlarged plot can be observed in Fig. 7b. The hydraulic force (F_{H}), chamber pressures (p_{A} and p_{B}), and the control signal sent to the valve (U_{C}) also demonstrate the good representativeness of the nonlinear dynamic model. In both simulation and experiment, the QFT-based prefilter and controller were used. The systems parameters are those presented in the Appendix.

The advantages of using HVE hoses for adding compliance to the system for improving the force control performance can be observed when comparing with the system using rigid pipes.

The controller $G(s)$ and prefilter $F(s)$ were designed for the case in which rigid pipes are used, assuming the same performance specifications applied to the system with hoses, resulting:

$$G(s) = \left(0.0005s + 0.002\right)/s, \tag{36}$$

and

$$F(s) = 484/(s^2 + 44s + 484). \tag{37}$$

Fig. 8 shows the system force simulation responses using pipes and hoses. A 4 kN step reference force was applied at 2 s. The disturbance input was a filtered step, used to reproduce a load movement disturbance, with 5 mm of magnitude at 3 s.

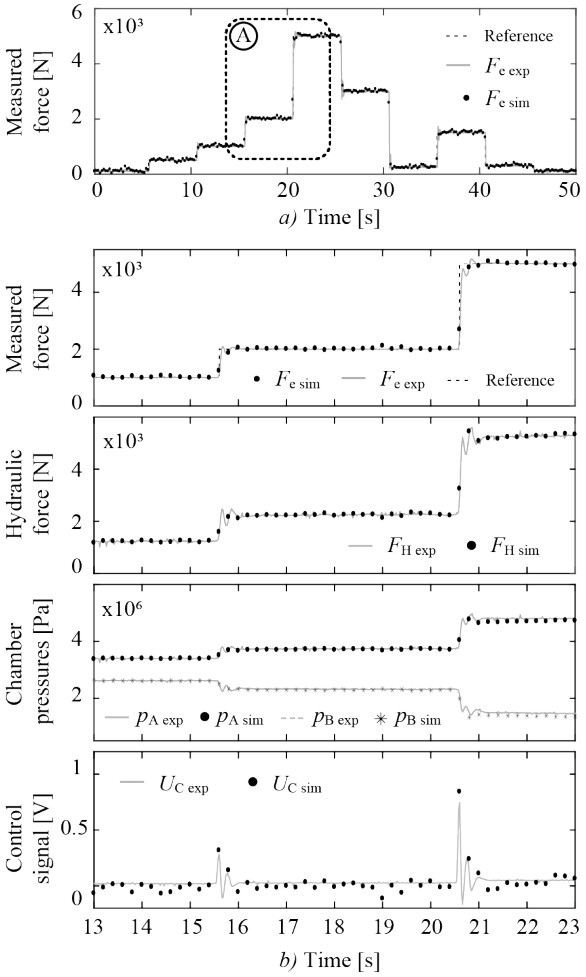

Fig. 7. *a) Comparison between experimental and simulated force tracking responses using HVE hoses, and b) enlarged plot of region A and hydraulic force, chamber pressures and control signal curves*

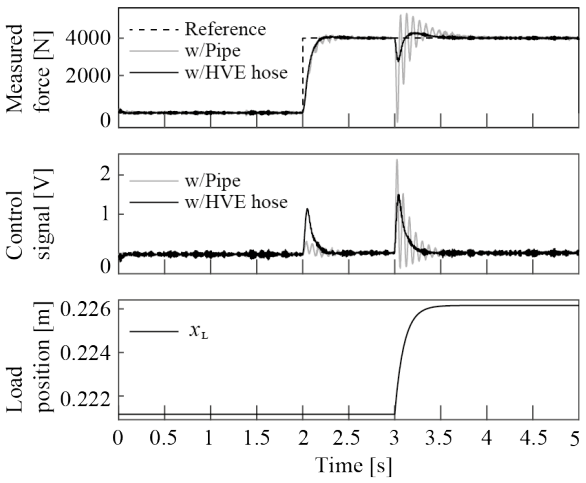

Fig. 8. *Comparison between force responses using pipes or HVE hoses*

The step response using rigid pipes was more oscillatory in comparison to the system with HVE hoses. The resulting overshoots were 3.87 % and 2.15 % and settling times ($t_{S1\%}$) equal to 0.33 s and 0.20 s, respectively. The settling time of the system with hoses is between the time domain specifications presented in section 4; however, the overshot is higher than 1%. The system with pipes was not able to strictly achieve the specifications using the designed QFT controller. It is necessary to observe that the QFT controller was designed based on the linear model considering the parameter uncertainties. Therefore, some deviation from the specifications can be expected.

The main drawback of a force control system is the disturbance rejection. As can be seen in Fig. 8, by reducing hydraulic stiffness through the use of HVE hoses, the output impedance is decreased, such that the load displacement causes small changes in the applied force. The control signal has a higher amplitude and is more oscillatory when using pipes, as expected, since there is not a hydraulic or mechanical compliant element.

6 CONCLUSIONS

A study on a hydraulic force control system using high volumetric expansion hoses to increase the hydraulic compliance was carried out. The major achievements of this study are to demonstrate the possibility of adding compliance hydraulically in order to perform the force control without using a spring and to establish an analytical procedure for selecting the hydraulic hoses necessary to achieve this goal. The inclusion of more hydraulic capacitive components allows a reduction in the effective bulk modulus and makes the system more compliant.

Based on the presented results, it was concluded that the force response performance of the system using hydraulically compliant components is improved in comparison to a system with rigid pipes. Moreover, the use of the QFT-based linear controller, applied in a nonlinear system, resulted in suitable performance and disturbance rejection capabilities.

Since the reduction in the hydraulic stiffness makes the system more compliant and conservative, the complexity of the controller is also reduced giving the perspective of the use of other types of controllers, including the classical PID.

Future work should include developing a selection procedure for accumulators with a focus on force control and series hydraulic damping analysis aimed at improving the force control performance of a PHEA-based system.

6 ACKNOWLEDGEMENTS

Special thanks to CNPq by the financial support and to M.S. Craig Borghesani from Terasoft, Inc. for providing the QFT Toolbox for this study.

7 REFERENCES

[1] Wang, J., Zhang, G., Zhang, H., Fuhlbrigge, T. (2008). Force control technologies for new robotic applications. *IEEE International Conference on Technologies for Practical Robot Applications*, p. 143-149, **DOI:10.1109/TEPRA.2008.4686689**.

[2] Parzer, H., Gattringer, H., Müller, A., Naderer, R. (2016). Robot force/position control combined with ILC for repetitive high speed applications. *International Conference on Robotics in Alpe-Adria Danube Region*, p. 12-19, **DOI:10.1007/978-3-319-49058-8_2**.

[3] Alleyne, A., Liu, R. (1999). On the limitations of force tracking control for hydraulic servosystems. *Journal of Dynamic Systems, Measurement, and Control*, vol. 121, no. 2, p. 184-190, **DOI:10.1115/1.2802453**.

[4] Whitney, D. (1985). Historical perspective and state of the art in robot force control. *IEEE International Conference on Robotics and Automation*, p. 262-268, **DOI:10.1109/ROBOT.1985.1087266**.

[5] Calanca, A., Muradore, R., Fiorini, P. (2016). A review of algorithms for compliant control of stiff and fixed-compliance robots. *IEEE/ASME Transactions on Mechatronics*, vol. 21, no. 2, p. 613-624, **DOI:10.1109/TMECH.2015.2465849**.

[6] Udai, A.D., Hayat, A.A., Saha, S.K. (2014). Parallel active/passive force control of industrial robots with joint compliance. *IEEE/RSJ International Conference on Intelligent Robots and Systems*, p. 4511-4516, **DOI:10.1109/IROS.2014.6943201**.

[7] Boaventura, T. (2013). *Hydraulic Compliance Control of the Quadruped Robot HyQ*. Ph.D. Thesis, University of Genova, Genova.

[8] Robinson, D.W. (2000). *Design and Analysis of Series Elasticity in Closed-loop Actuator Force Control*. Ph.D. Thesis, Massachusetts Institute of Technology, Massachusetts.

[9] Lee, Y.-F., Chu, C.-Y., Xu, J.-Y., Lan, C.-C. (2016). A humanoid robotic wrist with two-dimensional series elastic actuation for accurate force/torque interaction. *IEEE/ASME Transactions on Mechatronics*, vol. 21, no. 3, p. 1315-1325, **DOI:10.1109/TMECH.2016.2530746**.

[10] Losey, D.P., Erwin, A., McDonald, C.G., Sergi, F., O'Malley, M.K. (2016). A time domain approach to control of series elastic actuators: adaptive torque and passivity-based impedance control. *IEEE/ASME Transactions on Mechatronics*, vol. 21, no. 4, p. 2085-2096, **DOI:10.1109/TMECH.2016.2557727**.

[11] Xu, Y., Hollerbach, J.M., Ma, D. (1995). A Nonlinear PD controller for force and control transient control. *IEEE Control Systems*, vol. 15, no. 1, p. 15-21, **DOI:10.1109/37.341859**.

[12] Alleyne, A., Liu, R. (2000). A simplified approach to force control for electro-hydraulic systems. *Control Engineering Practice*, vol. 8, no. 12, p. 1347-1356, **DOI:10.1016/S0967-0661(00)00081-2**.

[13] Ahn, K.K., Truong, D.Q., Thanh, T.Q., Lee, B.R. (2008). Online self-tuning fuzzy porportional-integral-derivative control for hydraulic load simulator. *Proceedings of the Institution of Mechanical Engineers, Part I: Journal of Systems and Control Engineering*, vol. 222, no. 2, p. 81-95, **DOI:10.1243/09596518JSCE484**.

[14] Nakkarat, P., Kuntanapreeda, S. (2009). Observer-based backstepping force control of an electrohydraulic actuator. *Control Engineering Practice*, vol. 17, no. 8, p. 895-902, **DOI:10.1016/j.conengprac.2009.02.011**.

[15] Plummer, A.R. (2007). Robust electrohydraulic force control. *Proceedings of the Institution of Mechanical Engineers, Part I: Journal of Systems and Control Engineering*, vol. 221, no. 4, p. 717-731, **DOI:10.1243/09596518JSCE370**.

[16] Lamming, C.P.G., Plummer, A.R., Hillis, A.J. (2010). Analysis of robust electrohydraulic force control. *7th International Fluid Power Conference*, p. 1-12.

[17] Wells, D.L., Iversen, E.K., Davis, C.C., Jacobsen, S.C. (1990). An investigation of hydraulic actuator performance trade-offs using a generic model. *IEEE International Conference on Robotics and Automation,* p. 2168-2173, **DOI:10.1109/ROBOT.1990.126325**.

[18] Petersen, N.R. (2002). *Loading Assembly Having a Soft Actuator*. U.S. Patent 6.457.369 B1, World intellectual property organization, Geneva.

[19] Zoppi, M. (2013). *Method for Adapting Stiffness in a Variable Stiffness Actuator*. U.S. Patent 2013/0047596 A1, World intellectual property organization, Geneva.

[20] Houpis, C.H., Rasmussen, S.J. (1999). *Quantitative Feedback Theory: Fundamentals and Applications*. Marcel Dekker, New York.

[21] Pratt, G.A., Williamson, M.M., Dillworth, P., Pratt, J., Wright, A. (1997). Stiffness isn't everything. O. Khatib, J. K. Salisbury (eds.), *Experimental Robotics IV*, Springer, Berlin, p. 253-262, **DOI:10.1007/BFb0035216**.

[22] MOOG (2007). *760 Series - Servovalves - ISO 10372 Size 04. MOOG*. East Aurora, New York Catalog CDL6335 Rev G 500-213 807.

[23] Szpak, R., Ramos Filho, J.R.B., De Negri, V.J. (2010). Theoretical and experimental study of the matching between proportional valves and symmetric and asymmetric cylinders. *7th International Fluid Power*, p. 155-166.

[24] Gomes, S.C.P., da Rosa, V.S. (2003). A new approach to compensate friction in robotic actuators. *IEEE International Conference on Robotics and Automation*, p. 622-627, **DOI:10.1109/ROBOT.2003.1241663**.

[25] EATON Co. (2008). *Synflex Hose and Fittings Master Catalog,* Eden Prairie, Catalog E-HOOV-MC002-M.

[26] Parker Hannifin Corp. (2012). *Parflex® Thermoplastic & Fluoropolymer Products - Hose, Tubing, Fittings & Accessories,* Ravenna, Catalog CAT 4660.

[27] Johnston, D.N., Way, T.M., Cone, K.M. (2010). Measured dynamic properties of flexible hoses. *Journal of Vibration and Acoustics*, vol. 132, no. 2, p. 021011-1-021011-8, **DOI:10.1115/1.4000774**.

[28] Borghesani, C., Chait, Y., Yaniv, O. (2003). *The QFT Frequency Domain Control Design Toolbox: For use with Matlab*. User's Guide. Terasoft.

[29] ISO 10770-1:2009. *Hydraulic fluid power — Electrically modulated hydraulic control valves — Part 1: Test methods*

for four-port directional flow-control valves. International Organization for Standardization, Geneva.

8 APPENDIX

Table 3. *Technical data used for simulations*

Hydraulic power unit	$p_S = 7\times10^6$ Pa
	$p_T = 0$ Pa
	$\beta_e = 1.2\times10^9$ Pa
Double rod and double acting cylinder	Model: BOSCH REXROTH CGT3 MS2 50/22-500/Z1X/B1
	$L = 0.5$ m
	$A_u = 1.5833\times10^{-3}$ m^2
	$M = 13.1$ kg
4/3 closed center servovalve	Model: MOOG 760 C263-A
	K_{vp}*$= 3\times10^{-7}$ m^3/(s·Pa$^{0.5}$)@70×10^5 Pa
	K_{vinp}*$= 2.405\times10^{-9}$ m^3/(s·Pa$^{0.5}$)@70×10^5 Pa
	$U_n = 10$ VDC
	$\omega_{nv} = 1099$ rad/s @ ±40 % of opening valve
	$\xi_v = 0.9$ @ ± 40 % of opening valve
High volumetric expansion hose	Model: EATON Synflex ® 3130–08
	$D_{ho} = 12.7\times10^{-3}$ m
	$E = 1.56\times10^{-7}$ m^3/m @ 70×10^5 Pa
	$L_{ho} = 1.5$ m
Pipes	D_p: 10.5×10^{-3} m
	L_p: 0.5 m
Load cell	Model: HBM U2AD1-1t
	Maximum capacity: 9800 N
	$K_S = 9.8\times10^7$ N/m

* Obtained through experimental tests